J Biomol NMR (2017) 68:215–224
DOI 10.1007/s10858-017-0121-x

ARTICLE

Probing slow timescale dynamics in proteins using methyl ^{1}H CEST

Tairan Yuwen[1] · Rui Huang[1] · Lewis E. Kay[1,2]

Received: 13 April 2017 / Accepted: 8 June 2017 / Published online: 24 June 2017

Abstract Although ^{15}N- and ^{13}C-based chemical exchange saturation transfer (CEST) experiments have assumed an important role in studies of biomolecular conformational exchange, ^{1}H CEST experiments are only beginning to emerge. We present a methyl-TROSY ^{1}H CEST experiment that eliminates deleterious ^{1}H–^{1}H NOE dips so that CEST profiles can be analyzed robustly to extract methyl proton chemical shifts of rare protein conformers. The utility of the experiment, along with a version that is optimized for $^{13}CHD_2$ labeled proteins, is established through studies of exchanging protein systems. A comparison between methyl ^{1}H CEST and methyl ^{1}H CPMG approaches is presented to highlight the complementarity of the two experiments.

Keywords ^{1}H CEST · Methyl-TROSY · $^{13}CH_3$-/$^{13}CHD_2$-methyl labeling · ms timescale dynamics · Conformational exchange

Introduction

Methyl groups are powerful NMR reporters of protein structure, dynamics and function, in particular for high molecular weight complexes (Gelis et al. 2007; Rosenzweig and Kay 2014). This is due to a number of factors. First, methyl-based experiments are generally of high sensitivity, a phenomenon that derives from the three equivalent protons per probe. Second, rapid averaging about the methyl threefold axis narrows spectral linewidths, as does the placement of methyl groups at the ends of often long sidechains that leads to further averaging. Third, methyl groups are often at interfaces between oligomers in complexes and in the interior of protein cores where they are important reporters of structure and dynamics (Janin et al. 1988). Fourth, the underlying methyl spin physics enables a TROSY effect that leads to further line-narrowing and sensitivity gains (Tugarinov et al. 2003). Fifth, it is now possible to label any of the methyl groups of the 6 methyl containing residues in proteins as $^{13}CH_3$ and many as $^{13}CHD_2$ or $^{13}CH_2D$, opening up the possibility of performing a wide variety of different experiments (Kerfah et al. 2015; Tugarinov and Kay 2005). The utility of methyl groups in the study of protein motion is emphasized by the significant number of ^{1}H, ^{13}C and ^{2}H based methyl spin relaxation experiments that have been developed to measure protein dynamics with frequencies spanning over 12 orders of magnitude (Sheppard et al. 2010). Particularly important is the millisecond (ms) timescale window as many critical biological processes involve biomolecular conformations with lifetimes in this regime (Boehr et al. 2006; Henzler-Wildman and Kern 2007; Neudecker et al. 2012; Palmer et al. 2001; Sekhar et al. 2015). To this end methyl ^{13}C (Ishima et al. 1999; Korzhnev et al. 2004; Lundstrom et al. 2007) and ^{1}H (Yuwen et al. 2017) CPMG experiments as well as methyl ^{13}C CEST based schemes (Bouvignies and Kay 2012a; Rennella et al. 2015) have been reported for characterizing ms timescale motions where a highly populated and long lived (ground) state interconverts with a

Electronic supplementary material The online version of this article (doi:10.1007/s10858-017-0121-x) contains supplementary material, which is available to authorized users.

✉ Lewis E. Kay
kay@pound.med.utoronto.ca

[1] Departments of Molecular Genetics, Biochemistry and Chemistry, University of Toronto, Toronto, ON, Canada

[2] Program in Molecular Structure and Function, Hospital for Sick Children, Toronto, ON, Canada

sparsely populated and transiently formed (excited) conformer. Notably absent in the NMR toolkit, however, is a methyl ^{1}H CEST experiment for studying such processes. This is a significant omission because ^{1}H spins in general can be very useful reporters of conformational exchange, in part because of the sensitivity of proton chemical shifts to proximal aromatic moieties (Wuthrich 1986), and because methyl groups, in particular, are excellent probes of protein interiors (Janin et al. 1988) that often undergo significant structural changes during the exchange event.

Despite the obvious importance of ^{1}H methyl CEST, a difficulty with ^{1}H CEST, in general, has been that dips in CEST profiles arise from both chemical and dipolar (^{1}H–^{1}H cross relaxation) exchange and for applications to even moderately sized proteins the large number of NOE dips obscures the desired ones from chemical exchange (Bouvignies and Kay 2012b). We have recently shown that for ^{15}N labeled proteins amide ^{1}H CEST profiles can be generated that are completely free of NOE effects (Yuwen et al. 2017). This is achieved by exploiting the spin state of the attached ^{15}N to generate ^{15}N spin state selective ^{1}H profiles where the exchange dips, but not those derived from NOEs, are offset with respect to each other by the magnitude of the one bond ^{1}H–^{15}N scalar coupling, $^{1}J_{HN}$. In this way subtraction of the pair of CEST profiles corresponding to $^{15}N^{\alpha}$ and $^{15}N^{\beta}$, where α and β denote the up and down ^{15}N spin states respectively, results in a difference CEST profile where NOE artifacts are removed. In principle, the ^{13}C spin of the $^{13}CH_3$ labeled methyl group could be used in an analogous manner as the ^{15}N spin of the amide moiety, however, in practice the situation is complicated by the more complex AX_3 methyl spin system relative to the amide (AX) and by the fact that it is desirable to develop an experiment that benefits from the methyl-TROSY effect so as to optimize sensitivity. Here we describe such an experiment, along with the corresponding experiment for $^{13}CHD_2$ methyl groups, and present applications to exchanging protein systems to verify the methodology. We also highlight the relative strengths and weakness of methyl ^{1}H CEST versus methyl ^{1}H CPMG, emphasizing the importance of each class of experiment and their complementarity.

Materials and methods

Sample preparation

NMR samples of [U-^{15}N; U-^{2}H; Ileδ1-$^{13}CH_3$; Leu,Val-$^{13}CH_3/^{12}CD_3$]-labeled and [U-^{15}N; U-^{2}H; Ileδ1-$^{13}CHD_2$; Leu,Val-$^{13}CHD_2/^{13}CHD_2$]-labeled G48A Fyn SH3 were prepared as described previously (Bouvignies et al. 2014). Sample concentrations where 1.1 and 1.35 mM for $^{13}CH_3$- and $^{13}CHD_2$-labeled protein, dissolved in 50 mM sodium phosphate, 0.2 mM EDTA, 0.05% NaN_3, pH 7.0, 90%H_2O/10%D_2O. A 1.7 mM [U-^{15}N; U-^{2}H; Ileδ1-$^{13}CH_3$; Leu,Val-$^{13}CH_3/^{12}CD_3$; Met-$^{13}CH_3$] L99A T4L sample was generated following the protocol described by Bouvignies et al. (Bouvignies et al. 2011), using a 50 mM sodium phosphate, 25 mM NaCl, 2 mM EDTA, 2 mM NaN_3, pH 5.5, 100% D_2O buffer. Samples of the 'half proteasome' from *T. acidophilum* (Sprangers and Kay 2007), (referred to in what follows as $\alpha_7\alpha_7$, 360 kDa) were used to test the sensitivity of the pulse schemes of Fig. 1, to ensure that complete subtraction of NOE dips is achieved for high molecular weight systems and to evaluate the linewidths of major state dips as a function of the protein molecular weight. Samples comprised ~0.9 mM (monomer concentration) [U-^{2}H; Ileδ1-$^{13}CH_3$; Leu,Val-$^{13}CH_3/^{12}CD_3$; Met-$^{13}CH_3$]-labeled or [U-^{2}H; Ileδ1-$^{13}CHD_2$; Leu,Val-$^{13}CHD_2/^{13}CHD_2$; Met-$^{13}CH_3$]-labeled protein, 25 mM potassium phosphate pH 7.4, 50 mM NaCl, 4.6 mM NaN_3, 1 mM EDTA, 100% D_2O. The level of deuteration in all samples was >95% at all carbon sites.

NMR spectroscopy

^{1}H CEST datasets were recorded on $^{13}CH_3$- and $^{13}CHD_2$-labeled G48A Fyn SH3 using a 600 MHz Bruker spectrometer equipped with a gradient triple-axis cryogenically cooled probe, 25 °C. In studies of the $^{13}CH_3$ sample ^{1}H CEST datasets were recorded with the pulse scheme of Fig. 1a using weak B_1 fields of 26.1 and 42.2 Hz, T_{Ex} = 400 ms. Experiments were obtained as interleaved pseudo-4D datasets whereby a pair of spectra are recorded for each weak ^{1}H CEST field, varied over the range −1.0–1.5 ppm with step sizes of 25 (B_1 = 26 Hz) or 40 (B_1 = 42 Hz) Hz. These spectra are then manipulated to separate $IC^{I\alpha}$ and $IC^{I\beta}$ pathways (*i.e.*, the pathways derived from methyl ^{1}H magnetization coupled to ^{13}C with spin state α and β, respectively, see below). In addition a 2D reference dataset was recorded with a B_1 offset of −12 kHz, equivalent to setting B_1 = 0 Hz (Yuwen et al. 2017). This dataset was used to rescale the CEST baseline to 1.0 for each profile by plotting the ratio of major state cross-peak intensities, $I(T_{Ex},B_1)/I(T_{Ex},B_1=0)$, as a function of the position of the weak B_1 field (see CEST profiles, Figs. 2, 3, 4). Each 2D dataset was recorded with 4 transients/FID, a relaxation delay of 1.0 s and (640, 24) complex points in (t_2, t_1) to give a net acquisition time of ~5 min/spectrum. The net measurement time for each CEST dataset was ~11 h (B_1 = 26 Hz) or ~7 h (B_1 = 42 Hz). ^{1}H R_1 rates, used subsequently in fitting of the CEST profiles, were measured with a very similar pulse scheme to that of Fig. 1 with the exception that H_z magnetization was inverted prior to the T_{Ex} period in successive scans with modification of the phase cycle such that H_z effectively decays to zero during T_{Ex}.

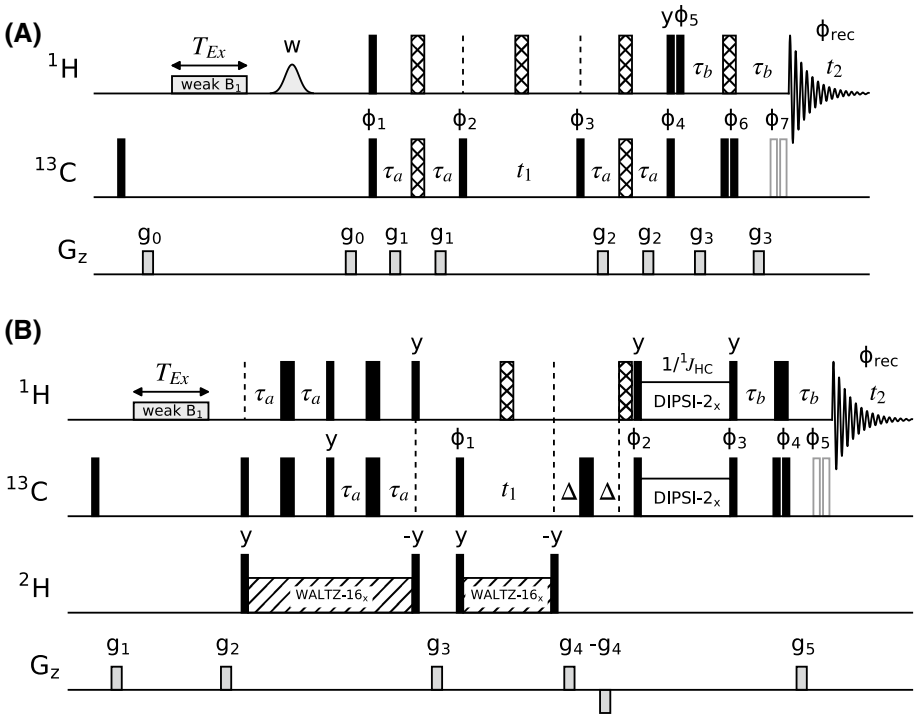

Fig. 1 **a** Methyl TROSY based pulse scheme for recording methyl ^{1}H CEST profiles. 90° (180°) rectangular pulses on ^{1}H and ^{13}C channels, denoted by *narrow (wide) rectangles*, are applied at maximum power. The *hatched rectangles* denote $90_x180_y90_x$ composite pulses (Levitt and Freeman 1979), while the water-selective shaped pulse marked with "w" (~7 ms) is implemented using an EBURP-1 profile (Geen and Freeman 1991). The final two 90° pulses on the ^{13}C channel (denoted by *narrow white rectangles*) are only required for the S^{3}E scheme (Felli and Pierattelli 2015), as described below. ^{1}H and ^{13}C carrier frequencies are set to the center of the methyl group region (~0.5, ~20 ppm), with the exception of during the CEST element where the ^{1}H carrier is placed at a frequency within the methyl range that is subsequently incremented with each CEST plane, and for the water selective pulse where the carrier is placed on resonance with the water line. After the t_1 period both $IC^{I\alpha}$ and $IC^{I\beta}$ pathways are retained and these are subsequently separated as described below. The delay $\tau_a \simeq 1/(4^1J_{HC})$ is set to 2.0 ms. All pulses are applied with phase x unless otherwise indicated. The following phase cycle is used: ϕ_1=y, −y, −y, y; ϕ_2=x, −x, −x, x; ϕ_3=4(x), 4(−x); ϕ_5=−y, y; with a minimum phase cycle of 2. Quadrature detection in F_1 is achieved by decrementing the phase of ϕ_1 by π/2 and incrementing the phase of ϕ_2 by π/2 simultaneously. Separation of $IC^{I\alpha}$ and $IC^{I\beta}$ pathways can be achieved using either IPAP (Ottiger et al. 1998; Yang and Nagayama 1996) (τ_b=1/(4$^1J_{HC}$)=2.00 ms) or S^{3}E (Felli and Pierattelli 2015) (τ_b=1/(8$^1J_{HC}$)) schemes, each with similar performance in terms of pathway selection. Note that a value of τ_b=1.03 ms was found to be optimal for the S^{3}E scheme in terms of isolating each of the two pathways. In the IPAP version ϕ_4=4(y), 4(−y); ϕ_6=−x; ϕ_{rec}=x, 2(−x), x, −x, 2(x), −x for recording in-phase (IP) spectra, while ϕ_4=4(−y), 4(y); ϕ_6=x; ϕ_{rec}=y, 2(−y), y, −y, 2(y), −y for recording anti-phase (AP) spectra. In the S^{3}E version a pair of datasets are recorded with ϕ_4=4(y), 4(−y); ϕ_6=x; ϕ_7=x; ϕ_{rec}=x, 2(−x), x, −x, 2(x), −x and with ϕ_4=4(−y), 4(y); ϕ_6=x; ϕ_7=−x; ϕ_{rec}=y, 2(−y), y, −y, 2(y), −y. In both IPAP and S^{3}E approaches the separately recorded datasets are added and subtracted to give CEST spectra corresponding to $IC^{I\alpha}$ and $IC^{I\beta}$ pathways. Gradients are applied with the following durations (ms) and strengths (in % maximum): g$_0$: (1.0, 50%), g$_1$: (0.5, 30%), g$_2$: (0.5, 30%), g$_3$: (0.5, 40%). The weak ^{1}H B_1 field was calibrated using the approach of Guenneugues et al. (1999). An alternative scheme which implements 3-9-19 WATERGATE (Sklenar et al. 1993) during the final IPAP/S^{3}E period achieves much higher water suppression and can be used for studying protein samples in H_2O-based solvent; in this case stronger g$_3$ gradients are used, (0.8, 80%). A small sensitivity loss (<10%) has been noted in studies of large proteins ($\alpha_7\alpha_7$) when the WATERGATE scheme is used. **b** Methyl ^{1}H-CEST experiment for measurement of slow chemical exchange processes in $^{13}CHD_2$-labeled proteins. Some of the details of this scheme are as in **a** and are not repeated. ^{2}H WALTZ-16 decoupling elements (Shaka et al. 1983) are applied with a field of 500 Hz, flanked by ~1.7 kHz pulses that minimize instabilities to the lock channel. Heteronuclear cross-polarization (duration $1/^1J_{HC} \simeq 8$ ms) is achieved with an ~8 kHz DIPSI-2 field (Shaka et al. 1988) applied to both ^{1}H and ^{13}C that transfers ^{13}C magnetization to ^{1}H magnetization in a spin state selective manner (Luy 2004; Yang and Kay 1999). The separation of $IC^{I\alpha}$ and $IC^{I\beta}$ pathways, that are recorded simultaneously, is achieved in a manner as described for the methyl-TROSY based scheme, exploiting either IPAP or S^{3}E elements. $\tau_a \simeq 1/(4^1J_{HC})$=2.0 ms. The following phase cycle is used: ϕ_1=x, −x; ϕ_2=y. Quadrature detection in F_1 is achieved by inverting the phase of ϕ_2 together with the sign of gradient g$_5$ (Kay et al. 1992; Schleucher et al. 1993). Separation of $IC^{I\alpha}$ and $IC^{I\beta}$ pathways can be achieved using either IPAP (Ottiger et al. 1998; Yang and Nagayama 1996) (τ_b=1/(4$^1J_{HC}$)=2.00 ms) or S^{3}E (Felli and Pierattelli 2015) (τ_b=1/(8$^1J_{HC}$)) schemes, each with similar performance levels in terms of pathway selection. Note that a value of τ_b=1.03 ms was found to be optimal for the S^{3}E scheme in terms of isolating each of the two pathways. In the IPAP version ϕ_3=y; ϕ_4=−x; ϕ_{rec}=x, −x for recording in-phase (IP) spectra, while ϕ_3=−y; ϕ_4=x; ϕ_{rec}=y, −y for recording anti-phase (AP) spectra. The final two90° pulses on the ^{13}C channel, denoted by *narrow white rectangles*, are only required for the S^{3}E scheme. Here a pair of datasets are recorded with ϕ_3=y; ϕ_4=x; ϕ_5=x; ϕ_{rec}=x, −x and with ϕ_3=−y; ϕ_4=x; ϕ_5=−x; ϕ_{rec}=y, −y. In both IPAP and S^{3}E approaches the separately recorded datasets are added and subtracted to generate CEST spectra corresponding to $IC^{I\alpha}$ and $IC^{I\beta}$ pathways. Gradients are applied with the following durations (ms) and strengths (in % maximum): g$_1$: (0.5, 30%), g$_2$: (0.5, 40%), g$_3$: (1.0, −50%), g$_4$: (0.512, 90%), g$_5$: (0.256, 90%)

^{1}H CEST experiments were recorded for $^{13}CHD_2$-labeled G48A Fyn SH3 using the scheme of Fig. 1b. Many experimental details are as above for the $^{13}CH_3$ sample and will not be repeated. Each 2D dataset was recorded with two transients/FID, a relaxation delay of 2.0 s, that takes into account the approximate twofold longer T_1 values relative to $^{13}CH_3$ labeling (where a relaxation delay of 1 s was used), see Figure S1, and (640, 24) complex points in (t_2, t_1) to give a net acquisition time of ~5 min/spectrum. The total measurement time for each pseudo-4D was ~11 h ($B_1 = 26$ Hz) or ~7 h ($B_1 = 42$ Hz), as for the experiments recorded on the $^{13}CH_3$ sample. ^{15}N CEST datasets, collected to validate the exchange parameters obtained via the ^{1}H CEST experiments, were measured using the standard pulse scheme described previously (Vallurupalli et al. 2012) with two different weak B_1 fields (22.7 and 36.1 Hz) and $T_{Ex} = 400$ ms.

A methyl-TROSY based ^{1}H CEST (Fig. 1a) dataset was measured for $^{13}CH_3$-labeled L99A T4L using a 800 MHz Bruker spectrometer equipped with a z-axis cryogenically cooled probe, 8.8 °C and a weak B_1 field of 30.4 Hz, $T_{Ex} = 500$ ms. Experiments were collected by varying the position of the weak ^{1}H CEST field during T_{Ex} over a range extending from −1.5 to 2.3 ppm in step sizes of 30 Hz. Each 2D dataset was recorded with 2 transients/FID, a relaxation delay of 0.5 s and (768, 80) complex points in (t_2, t_1) to give a net acquisition time of ~6 min/spectrum. The net measurement time for each CEST dataset was ~20 h.

A methyl-TROSY based ^{1}H CEST (Fig. 1a) dataset was recorded on $\alpha_7\alpha_7$, 600 MHz, 50 °C using a weak B_1 field of 32.1 Hz, $T_{Ex} = 400$ ms. The position of the weak ^{1}H CEST field was varied over a range extending from −0.7 to 2.1 ppm in step sizes of 30 Hz. Each 2D dataset was recorded with two transients/FID, a relaxation delay of 1 s and (640, 64) complex points in (t_2, t_1) to give a net acquisition time of ~6 min/spectrum and a net measurement time of ~14 h. A similar experiment (Fig. 1b) was recorded using the $^{13}CHD_2$-labeled complex except that the relaxation delay was increased to 2 s.

^{1}H methyl TQ CPMG datasets (Yuwen et al. 2016) were recorded at 600 and 800 MHz, 25 °C, on a $^{13}CH_3$-labeled L99A T4L sample using a constant-time CPMG relaxation element of duration $T_{relax} = 10$ ms, 18 ν_{CPMG} values were sampled in the range of 100–2000 Hz, where $\nu_{CPMG} = 1/(2\delta)$, and δ is the time between successive refocusing pulses. A net measurement time ~20 h was used for each CPMG dataset.

Data analysis

All NMR spectra were processed and analyzed using the *NMRPipe* suite of programs (Delaglio et al. 1995) with peak intensities extracted with the *autofit* subroutine. Prior to the calculation of difference ^{1}H-CEST profiles each of the $IC^{I\alpha}$ and $IC^{I\beta}$ CEST curves was first rescaled to bring the baseline position to 1.0. This is achieved by plotting the ratio $I(T_{Ex},B_1)/I(T_{Ex},B_1 = 0)$ as a function of the position of the weak B_1 field. The difference ^{1}H CEST profile ($IC^{I\alpha}$–$IC^{I\beta}$) was then fitted to extract exchange parameters and chemical shift differences for G48A Fyn SH3 or only shift differences for L99A T4L (Yuwen et al. 2017). The analyses of CEST profiles were carried out using the software package *ChemEx* (https://github.com/gbouvignies/chemex); a separate module is required for fitting the difference ^{1}H-CEST profiles which is available upon request. In total 12 and 11 CEST profiles were selected for G48A Fyn SH3 and L99A T4L, respectively, to extract $\Delta\varpi$ values. For G48A Fyn SH3, only three CEST profiles with distinct minor and major dips were chosen to estimate (p_E, k_{ex}). Exchange parameters were not estimated for L99A T4L from ^{1}H CEST because of the influence of ^{1}H–^{1}H cross relaxation on the extracted values (Yuwen et al. 2017). No minor state dips were observed in CEST datasets measured on $\alpha_7\alpha_7$. Datasets were recorded to establish that clean difference profiles (i.e., no NOE dips) could be obtained over a wide range of different molecular weight protein systems that might be studied with this methodology and to evaluate the linewidths of major state dips in difference CEST profiles ($^{13}CH_3$-sample).

For the analysis of CPMG datasets that were recorded for L99A T4L, effective transverse relaxation rates, $R_{2,eff}$, were calculated based on peak intensities according to the relation $R_{2,eff}(\nu_{CPMG}) = -\ln(I(\nu_{CPMG})/I_0)/T_{relax}$, where I_0 is the peak intensity in a reference spectrum recorded without the relaxation delay, T_{relax} (Mulder et al. 2001). The fitting of CPMG datasets was carried out with *ChemEx*, following previously described protocols (Yuwen et al. 2016). Initially 9 residues with significant CPMG dispersion profiles (>10 s^{-1} at 600 MHz) were selected to estimate (p_E, k_{ex}) values that were then fixed in fits of 42 dispersion curves.

Results and discussion

Figure 1a shows the methyl-TROSY based ^{1}H CEST pulse scheme that has been developed to probe chemical exchange. Key to the approach is that ^{1}H longitudinal magnetization coupled to $^{13}C^{\alpha}$ ($I_zC^{I\alpha}$) and $^{13}C^{\beta}$ ($I_zC^{I\beta}$) during the initial CEST element is detected as $I_{TR}C^{I\alpha}$ and $I_{TR}C^{I\beta}$, respectively, at the end of the pulse scheme, with the subscript *TR* denoting transverse magnetization. The two magnetization pathways, $I_zC^{Ij} \rightarrow I_{TR}C^{Ij}, j \in (\alpha, \beta)$, are preserved in a single scan and then separated prior to detection (t_2), thus improving sensitivity by a factor of $\sqrt{2}$ over sequences where only one of the two pathways is recorded.

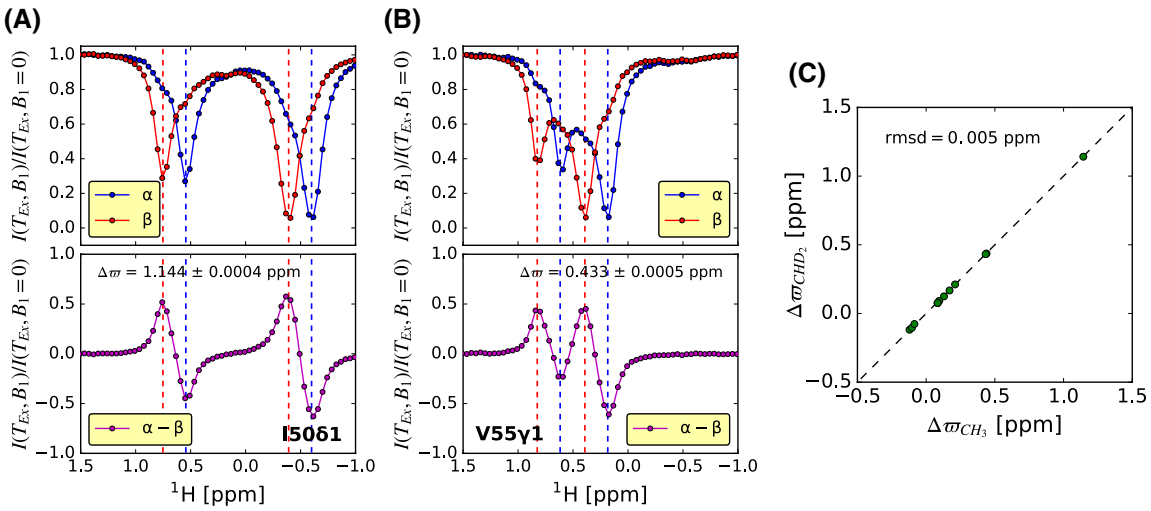

Fig. 2 a, b Representative spin state selective methyl ^{1}H CEST profiles (*top*) and difference profiles (*bottom*) measured on a $^{13}CH_3$-labeled G48A Fyn SH3 sample using the scheme of Fig. 1a, 25 °C, 600 MHz, T_{Ex} = 400 ms, weak B_1 field = 26.1 Hz. The ratio $I(T_{Ex},B_1)/I(T_{Ex},B_1=0)$ (y-axis) is plotted as a function of the position of the weak B_1 field (x-axis) where $I(T_{Ex},B_1)$ and $I(T_{Ex},B_1=0)$ are the intensities of the major state peak when the field is set to B_1 and to 0 (or alternatively when the field is far removed from any resonance, see Materials and methods), respectively. The positions of ground and excited states are indicated with *dashed lines* in *blue* or *red* for ^{13}C spin state α or β respectively. Values of $\Delta\varpi$ obtained from fits are indicated in each panel. **c** Linear correlation plot of $\Delta\varpi$ values obtained via methyl CEST experiments recorded using the pulse schemes of Fig. 1a ($^{13}CH_3$), b ($^{13}CHD_2$). Note that the uncertainties in $\Delta\varpi$ are smaller than the sizes of the data points in the plot. Details regarding optimal recording of both classes of methyl CEST experiment are provided in Figure S3

In order to illustrate a number of key aspects of this pulse scheme we present a brief description of the magnetization flow, neglecting pulse imperfections and relaxation and assuming that $\tau_a = 1/(4\,{}^1J_{HC})$, where ${}^1J_{HC}$ is the one bond ^{1}H–^{13}C scalar coupling constant. Focusing initially on longitudinal ^{1}H magnetization, $I_z(1 \pm 2C_z)$, and on only the first line of the phase cycle indicated in the legend to Fig. 1a, it follows that

$$\begin{aligned} I_z^j(1 \pm 2C_z) \rightarrow\ & 2I_x^jC_y\cos(\omega_c t_1) - 2I_x^jC_x\sin(\omega_c t_1) \\ & \mp 8I_y^jC_xI_z^kI_z^l\cos(\omega_c t_1) \mp 8I_y^jC_yI_z^kI_z^l\sin(\omega_c t_1) \end{aligned} \quad (1)$$

where the right hand side contains the relevant magnetization terms at the end of the t_1 period, with the superscripts *j,k,l* distinguishing the three identical protons, I_i and C_i denote ^{1}H and ^{13}C ($i \in \{x, y, z\}$) magnetization and ω_c is the ^{13}C precession frequency. Note that all terms on the right hand side of Eq. (1) contain ^{1}H–^{13}C double/zero quantum elements. In the absence of the ^{1}H 180° pulse in the center of the t_1 period, and neglecting ^{1}H chemical shift evolution, each of these elements would evolve into three resolved multiplet components due to scalar coupling, separated from each other by ${}^1J_{HC}$; the middle component relaxes slowly while the outer components are fast relaxing and typically decay during the course of the pulse scheme (Tugarinov et al. 2003). Immediately after the ^{13}C pulse of phase ϕ_4, and neglecting the simultaneous ^{1}H $90_y90_{\phi5}$ pulses for the moment, the terms of interest are

$$I_y^j(1 \pm 2C_z)\cos(\omega_c t_1) - 4I_x^jI_z^kI_z^l(1 \pm 2C_z)\sin(\omega_c t_1) \quad (2)$$

The second term in Eq. (2) is problematic. During the subsequent $2\tau_b$ period and the following t_2 evolution intra-methyl ^{1}H–^{1}H dipolar cross-correlated relaxation partially converts it to $I_x^j(1 \pm 2C_z)$ that leads to phase anomalies in peak lineshapes. This problem can be circumvented by the application of a ^{1}H 90_y purge pulse or by applying a ^{1}H 180° pulse in alternate scans ($90_y90_{\phi5}$) simultaneously with the ^{13}C $90_{\phi4}$ pulse; the purge pulse ensures that the undesired magnetization becomes non-observable while the ^{1}H $90_y90_{\phi5}$ pulse pair inverts the undesired magnetization in successive scans so that it can be removed by phase cycling. We prefer the latter approach, as this preserves the methyl-TROSY effect, while a ^{1}H 90° pulse will partially interconvert fast and slowly relaxing ^{1}H components, that leads to reduced sensitivity and resolution in the resulting datasets (Tugarinov et al. 2003). The remaining element of duration $2\tau_b$ separates the $I_y^j(1 \pm 2C_z)$ components according to the ^{13}C spin state to generate the $IC^{l\alpha}$ and $IC^{l\beta}$ CEST profiles. Despite the increased number of pulses and delays relative to a standard HMQC scheme the sensitivity of this new experiment is high, with relative peak intensities ranging between 90–95% and 80–85% for applications to Fyn SH3 (7 kDa, 25 °C) and $\alpha_7\alpha_7$ (360 kDa, 50 °C), respectively. Note that because spin state selective datasets are recorded the comparison we have made is to an F_2-coupled

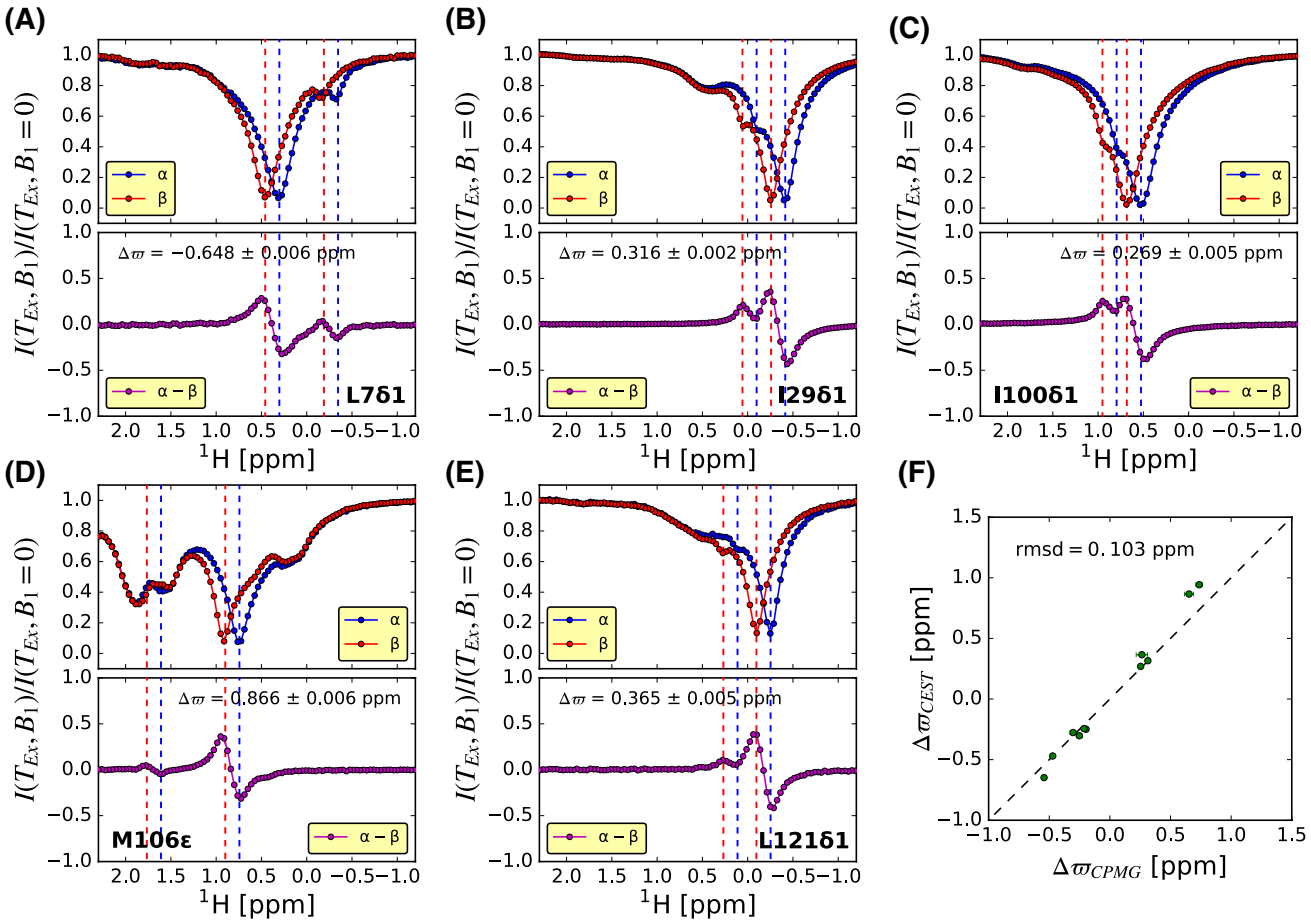

Fig. 3 **a**–**e** Representative spin state selective methyl ^{1}H CEST profiles (*top*) and difference profiles (*bottom*) measured on a $^{13}CH_3$-labeled L99A T4L sample using the scheme of Fig. 1a, 9 °C, 800 MHz, T_{Ex} = 500 ms, weak B_1 field = 30.4 Hz. **f** Linear correlation plot of $\Delta\varpi$ values obtained from analyses of methyl ^{1}H CEST and methyl ^{1}H TQ-CPMG experiments (Yuwen et al. 2016) (25 °C); uncertainties in $\Delta\varpi_{CEST}$ values are smaller than the sizes of data points in the plot

HMQC; there is, of course, a penalty of a factor of 2 that takes into account the fact that a pair of sub-spectra are recorded, one for each of the ^{13}C spin states, as there would be in a coupled HMQC dataset as well.

Figure 1b illustrates the pulse scheme for recording methyl ^{1}H CEST profiles when $^{13}CHD_2$ labeling is used. In this case the approach is essentially identical to that described previously for amide protons (Yuwen et al. 2017), with the exception that in the present implementation we have used heteronuclear cross-polarization to transfer magnetization back to ^{1}H for detection in an enhanced sensitivity manner (Kay et al. 1992; Schleucher et al. 1993).

As a first step in validating the methyl ^{1}H-CEST experiment we recorded CEST profiles (scheme Fig. 1a) on a [U-^{15}N; U-^{2}H; Ileδ1-$^{13}CH_3$; Leu,Val-$^{13}CH_3$/$^{12}CD_3$]-labeled G48A Fyn SH3 domain (25 °C) that has been shown previously to interconvert between dominant folded and rare unfolded states, via a two-step exchange process, $G \underset{k_{EG}}{\overset{k_{GE}}{\rightleftarrows}} E$ (Di Nardo et al. 2004). Figure 2a, b shows representative profiles for two methyl groups from G48A Fyn SH3, along with difference profiles that remove any NOE dips. We have also recorded ^{1}H CEST profiles using a [U-^{15}N; U-^{2}H; Ileδ1-$^{13}CHD_2$; Leu,Val-$^{13}CHD_2$/$^{13}CHD_2$]-labeled sample with the pulse scheme of Fig. 1b that is optimized for $^{13}CHD_2$ methyl groups. Good agreement is obtained between extracted methyl ^{1}H chemical shift differences, $\Delta\varpi = \varpi_E - \varpi_G$ (ppm), Fig. 2c, and between exchange parameters (p_E, $k_{ex} = k_{EG} + k_{GE}$) = (8.4 ± 0.1%, 111.4 ± 3.5 s^{-1}), (7.6 ± 0.1%, 106.2 ± 2.4 s^{-1}) and (8.3 ± 0.1%, 104.5 ± 1.6 s^{-1}) obtained from $^{13}CH_3$-^{1}H CEST, $^{13}CHD_2$-^{1}H CEST and ^{15}N based experiments. As discussed previously, exchange parameters become increasingly compromised in ^{1}H CEST experiments as ^{1}H–^{1}H cross relaxation becomes more significant (Yuwen et al. 2017); for applications to small, highly deuterated proteins such as the Fyn SH3 domain (7 kDa) considered here this effect is relatively minor and robust exchange parameters can be fitted. In general,

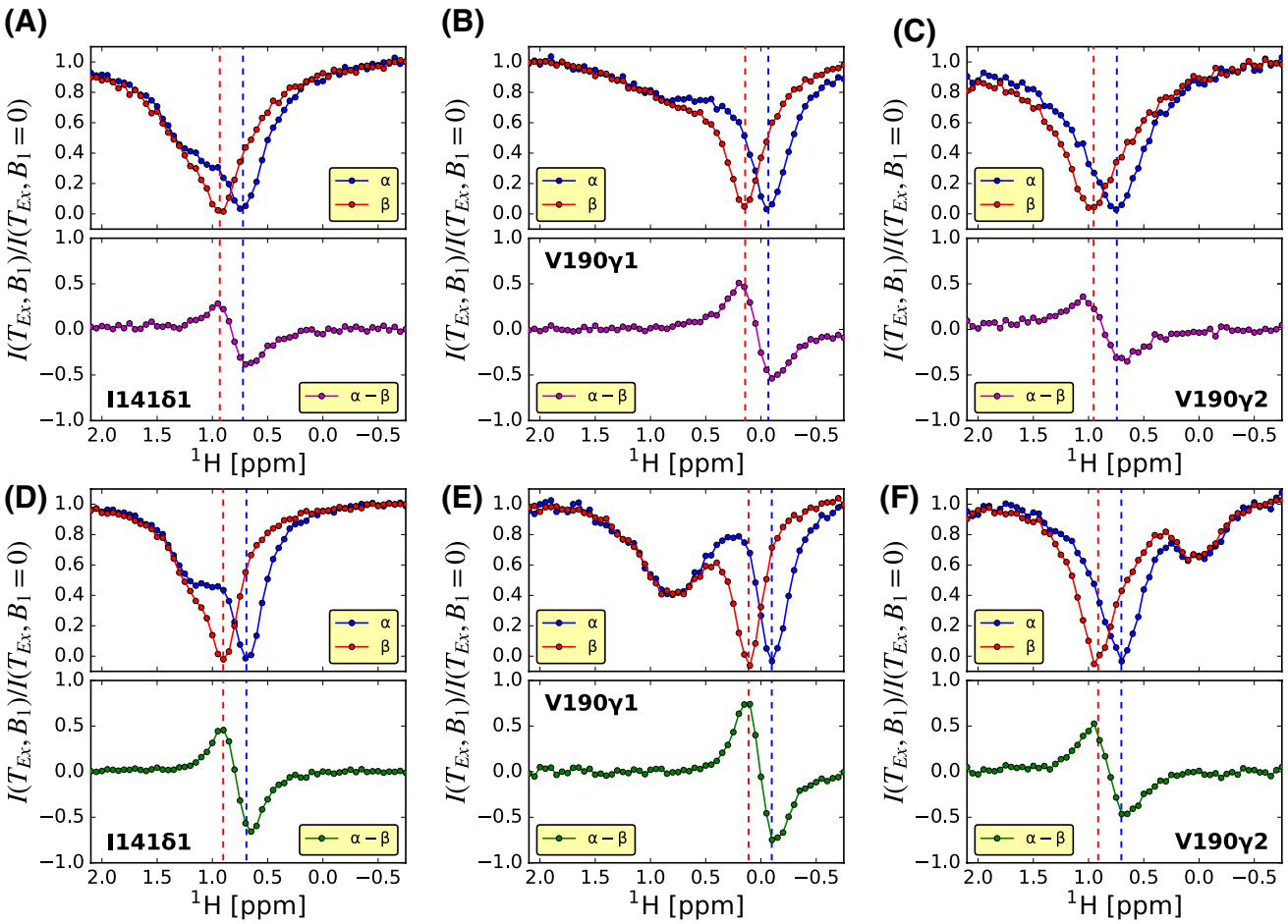

Fig. 4 **a–c** Representative spin state selective methyl ^{1}H CEST profiles (*top*) and difference profiles (*bottom*) measured on a $^{13}CH_3$-labeled $\alpha_7\alpha_7$ sample using the scheme of Fig. 1a, 50 °C, 600 MHz, T_{Ex} = 400 ms, weak B_1 field = 32.1 Hz. **d–f** As in **a–c** but for a $^{13}CHD_2$-labeled $\alpha_7\alpha_7$ sample obtained using the scheme of Fig. 1b. Additional dips for Leu/Val residues are found in difference profiles of the $^{13}CHD_2$-labeled sample (e.g., **e, f** as for V190γ1/γ2) due to ^{1}H–^{1}H NOEs between the two isopropyl $^{13}CHD_2$ methyl groups in a given residue (note that the $^{13}CH_3$ sample has $^{13}CH_3/^{12}CD_3$ methyl labeling)

however, it is preferable to obtain (p_E, k_{ex}) values from ^{15}N experiments for which cross relaxation is not an issue (Yuwen et al. 2017).

Although $^{13}CH_3$ methyl labeling of proteins is more common than $^{13}CHD_2$ labeling, so that the methyl TROSY ^{1}H CEST experiment of Fig. 1a is likely to be more useful than the $^{13}CHD_2$ version (Fig. 1b), we were interested in comparing the relative signal to noise values (S/N) in both experiments to see where the advantage lies in terms of sensitivity. Notably S/N values were approximately 1.5–2 fold higher for Leu and Val and 2.5 fold higher for Ile in $^{13}CH_3$ datasets recorded on G48A Fyn SH3 when T_{Ex} is set to 0, Figure S1. We have also compared relative intensities of minor state CEST dips in difference datasets recorded on the $^{13}CH_3$- and $^{13}CHD_2$-labeled samples with T_{Ex} = 400 ms, focusing only on residues with large $\Delta\omega$ values so that accurate ratios could be quantified. Relative S/N values of 1.0 for Leu/Val and 1.8 for Ile are obtained ($^{13}CH_3/^{13}CHD_2$) that are smaller compared with T_{Ex} = 0 ms. This decrease reflects the faster ^{13}C longitudinal relaxation rates for $^{13}CH_3$ methyls relative to their $^{13}CHD_2$ counterparts (~2 vs. 1 s^{-1}) (Rennella et al. 2015) and the fact that ^{13}C spin flips during the CEST delay interconvert $I_zC^{I\alpha}$ and $I_zC^{I\beta}$, leading to an attenuation of the dips observed in the difference CEST profiles, as described previously (Yuwen et al. 2017). Although we have not compared S/N values for larger molecules, our previous studies focusing on very similar pulse sequences and identical labeling schemes to the ones compared here established a preference for $^{13}CH_3$ labeling and methyl-TROSY based experiments in applications to the 360 kDa half-proteasome (Religa and Kay 2010).

Having established the utility of ^{1}H methyl CEST in applications to small proteins we next turned to the L99A cavity mutant of T4 lysozyme (L99A T4L), labeled as [U-^{15}N; U-^{2}H; Ileδ1-$^{13}CH_3$; Leu,Val-$^{13}CH_3/^{12}CD_3$; Met-$^{13}CH_3$]

(Eriksson et al. 1992). L99A T4L interconverts between a ground state conformation where a 150 Å^3 cavity in the protein interior, formed by the L99A substitution, is empty and a conformation where the cavity is occupied by F114 (Bouvignies et al. 2011). Figure 3a–e highlights a number of CEST profiles recorded with the scheme of Fig. 1a (9 °C, correlation time 19 ns) and it is now clear that NOE dips can completely obscure the minor state CEST dips of interest in the spin state selective traces (see panel d, in particular). Nevertheless the NOE dips are removed cleanly in the difference traces, allowing the extraction of ^{1}H methyl $\Delta\varpi$ values so long as they exceed ~0.2 ppm. An excellent correlation between such values and corresponding shift differences from ^{1}H triple-quantum (TQ) CPMG experiments (25 °C) (Yuwen et al. 2016) is illustrated in Fig. 3f.

Although we expect that the ^{1}H methyl CEST methodology described here will have important applications to studies of slow timescale dynamics in high molecular weight complexes we do not presently have an appropriate large system that shows exchange in the CEST window. Nevertheless, we have recorded a CEST experiment on $\alpha_7\alpha_7$ as a control to ensure that clean separation of NOE and chemical exchange dips are obtained in difference CEST profiles in the case of very large protein systems as well. Figure 4 illustrates representative spin state selective ^{1}H CEST profiles for several residues, measured with the sequences of Fig. 1. The resulting difference profiles show only major state dips and establish the complete subtraction of NOEs, as expected. We were also interested in exploring how the linewidths of the major state CEST dips vary with molecular weight, as this is a critical parameter for estimating the lower bound of $\Delta\omega$ values that can be measured. Figure S2 shows the distribution of linewidths obtained for L99A T4L (correlation time of 19 ns, 9 °C) and $\alpha_7\alpha_7$ (125 ns, 50 °C), along with a schematic illustrating how we have defined linewidth in the context of the anti-phase lineshapes obtained in the difference CEST spectra. The linewidths of $\alpha_7\alpha_7$ are ~15% larger, on average, than those of L99A T4L, strongly suggesting that the methodology presented will be applicable in studies of high molecular weight systems, at least for those that are reasonably well behaved.

With the recent development of a sensitive methyl ^{1}H CPMG experiment that exploits ^{1}H TQ coherences during the CPMG relaxation element (Yuwen et al. 2016) and the introduction of methyl ^{1}H CEST here, it is of interest to compare the relative strengths of the two approaches. Although both experiments can provide detailed information on the exchanging system studied, they are optimally sensitive to different exchange regimes, as with CEST and CPMG in general (Sekhar and Kay 2013). For example, ^{15}N CEST studies of L99A at 9 °C establish that (p_E, k_{ex}) = (1.8 ± 0.01%, 215 ± 5 s^{-1}), so that maximum dispersion profile sizes are only ~4 s^{-1} ($p_E \times k_{ex}$, obtained in the slow exchange limit (Millet et al. 2000)), complicating robust analyses of CPMG data. Yet this slow exchange regime is ideal for CEST applications. Conversely, (p_E, k_{ex}) = (3.1 ± 0.1%, 1290 ± 50 s^{-1}) at 25 °C is optimal for CPMG but the rapid exchange rate leads to very significant line broadening for the minor state peaks (up to as much as 1250 s^{-1} = $(1-p_E)\times k_{ex}$, calculated in the slow exchange limit) that would render them invisible in CEST profiles. In this regard, CEST and CPMG are highly complementary and the utility of one method over the other depends on the exchange regime of the interconverting system of interest. Although it is tempting to argue that by manipulating the sample one can always change the exchange timescale so that one of the methods becomes preferable, in practice this is often not realized since exchange rates depend very significantly on the activation enthalpy for the interconversion, for example, when temperature is used as the variable.

L99A T4L is, in fact, an example of where it is possible to modify the exchange timescale by temperature so that both CEST and CPMG experiments can be made amenable to explore conformational exchange, albeit at different temperatures that tune k_{ex} to the appropriate values for each technique. As such it is possible to compare ^{1}H methyl CEST (9 °C) and ^{1}H methyl TQ CPMG (25 °C) profiles to illustrate the relative strengths of each method, Fig. 5. For the case of L7δ1 where $\Delta\varpi = -0.6$ ppm there is a large spacing between major and minor state dips in the CEST profile and the position of the minor state dip can be accurately established, by inspection, or by a single residue fit. In contrast, the large shift difference leads to a CPMG profile that decays only partially over the applied 2 kHz ν_{CPMG} range, challenging the accurate extraction of chemical shifts from fits of this profile in isolation or even globally (all fits were global). Note that in the TQ CPMG experiment the effective $\Delta\omega$ is three fold larger than for the corresponding single-quantum version (Tugarinov and Kay 2007) so that $\Delta\omega_{eff}$ = 7300 rad s^{-1} (at 600 MHz) $\gg k_{ex}$ = 1250 s^{-1} in this example. For smaller chemical shift differences, on the order of 0.3 ppm, such as the case for I29δ1, there remains sufficient separation between major and minor CEST dips so that accurate $\Delta\varpi$ values can be obtained from the CEST experiment. The smaller $\Delta\varpi$ value leads to a more favorable situation for CPMG profiles as the effects of exchange can now be attenuated much more completely as a function of the pulsing rate. In contrast, as $\Delta\varpi$ values decrease further, to 0.06 ppm for L32δ2, there is insufficient resolution between major and minor dips in the difference CEST profile to measure $\Delta\varpi$. Because triple-quantum coherences are evolved during the CPMG element the effective $\Delta\varpi$ is scaled by three-fold so that large dispersion profiles are obtained for L32δ2 and the exchange timescale is slowed, enabling a proper analysis in this case. Of course, an advantage of CEST, in general, is that the sign of $\Delta\varpi$ is available

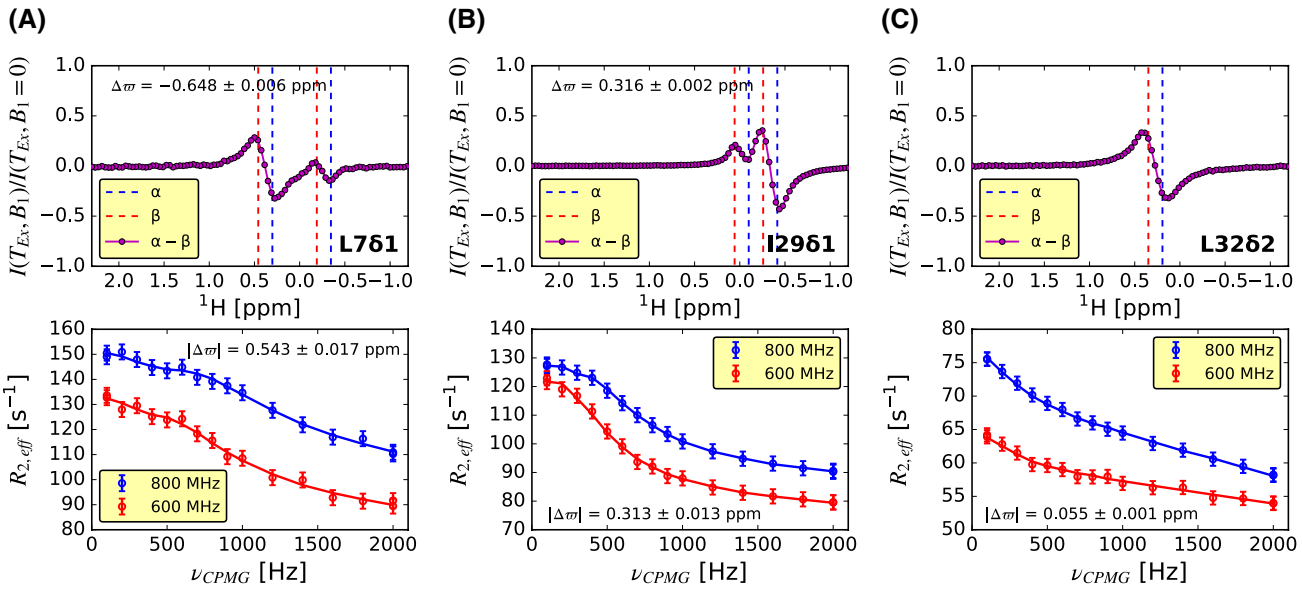

Fig. 5 Comparison of methyl ^{1}H CEST (9 °C) and methyl ^{1}H TQ-CPMG (25 °C) profiles for three different residues of L99A T4L, emphasizing the complementarity of the different experiments, as described in the text. In the CPMG profiles the effective relaxation rate, $R_{2,eff}$ is plotted as a function of the pulse repetition rate, defined in Materials and methods

by inspection, while additional experiments must be performed in the case of CPMG measurements to obtain this information (Skrynnikov et al. 2002).

In summary, we have presented methyl ^{1}H CEST experiments for studies of exchange dynamics in $^{13}CH_3$- and $^{13}CHD_2$-labeled proteins that completely eliminate deleterious NOE dips. The pulse schemes are complementary to methyl ^{1}H CPMG experiments because the CEST approach is optimally sensitive to exchange in a regime where CPMG dispersion profiles are small and not amenable for detailed analysis. The development of a large suite of different experiments, each with their own set of strengths, increases the range of important conformational exchange processes that can be studied by NMR and ultimately our insight into how excursions to rare conformational states impact biomolecular function.

Acknowledgements This work was supported by Grants from the Canadian Institutes of Health Research and the Natural Sciences and Research Council of Canada. L.E.K holds a Canada Research Chair in Biochemistry.

References

Boehr DD, McElheny D, Dyson HJ, Wright PE (2006) The dynamic energy landscape of dihydrofolate reductase catalysis. Science 313:1638–1642. doi:10.1126/science.1130258

Bouvignies G, Kay LE (2012a) A 2D ^{13}C-CEST experiment for studying slowly exchanging protein systems using methyl probes: an application to protein folding. J Biomol NMR 53:303–310. doi:10.1007/s10858-012-9640-7

Bouvignies G, Kay LE (2012b) Measurement of proton chemical shifts in invisible states of slowly exchanging protein systems by chemical exchange saturation transfer. J Phys Chem B 116:14311–14317. doi:10.1021/jp311109u

Bouvignies G et al (2011) Solution structure of a minor and transiently formed state of a T4 lysozyme mutant. Nature 477:111–114. doi:10.1038/nature10349

Bouvignies G, Vallurupalli P, Kay LE (2014) Visualizing side chains of invisible protein conformers by solution NMR. J Mol Biol 426:763–774. doi:10.1016/j.jmb.2013.10.041

Delaglio F, Grzesiek S, Vuister GW, Zhu G, Pfeifer J, Bax A (1995) NMRPipe: a multidimensional spectral processing system based on Unix pipes. J Biomol NMR 6:277–293. doi:10.1007/Bf00197809

Di Nardo AA, Korzhnev DM, Stogios PJ, Zarrine-Afsar A, Kay LE, Davidson AR (2004) Dramatic acceleration of protein folding by stabilization of a nonnative backbone conformation. Proc Natl Acad Sci USA 101:7954–7959. doi:10.1073/pnas.0400550101

Eriksson AE, Baase WA, Wozniak JA, Matthews BW (1992) A cavity-containing mutant of T4 lysozyme is stabilized by buried benzene. Nature 355:371–373. doi:10.1038/355371a0

Felli IC, Pierattelli R (2015) Spin-state-selective methods in solution- and solid-state biomolecular ^{13}C NMR. Prog Nucl Magn Reson Spectrosc 84:1–13. doi:10.1016/j.pnmrs.2014.10.001

Geen H, Freeman R (1991) Band-selective radiofrequency pulses. J Magn Reson 93:93–141. doi:10.1016/0022-2364(91)90034-Q

Gelis I et al (2007) Structural basis for signal-sequence recognition by the translocase motor SecA as determined by NMR. Cell 131:756–769. doi:10.1016/j.cell.2007.09.039

Guenneugues M, Berthault P, Desvaux H (1999) A method for determining B_1 field inhomogeneity. Are the biases assumed in heteronuclear relaxation experiments usually underestimated? J Magn Reson 136:118–126. doi:10.1006/jmre.1998.1590

Henzler-Wildman K, Kern D (2007) Dynamic personalities of proteins. Nature 450:964–972. doi:10.1038/nature06522

Ishima R, Louis JM, Torchia DA (1999) Transverse ^{13}C relaxation of CHD_2 methyl isotopmers to detect slow conformational changes

of protein side chains. J Am Chem Soc 121:11589–11590. doi:10.1021/ja992836b
Janin J, Miller S, Chothia C (1988) Surface, subunit interfaces and interior of oligomeric proteins. J Mol Biol 204:155–164. doi:10.1016/0022-2836(88)90606-7
Kay LE, Keifer P, Saarinen T (1992) Pure absorption gradient enhanced heteronuclear single quantum correlation spectroscopy with improved sensitivity. J Am Chem Soc 114:10663–10665. doi:10.1021/ja00052a088
Kerfah R, Plevin MJ, Sounier R, Gans P, Boisbouvier J (2015) Methyl-specific isotopic labeling: a molecular tool box for solution NMR studies of large proteins. Curr Opin Struct Biol 32:113–122. doi:10.1016/j.sbi.2015.03.009
Korzhnev DM, Kloiber K, Kay LE (2004) Multiple-quantum relaxation dispersion NMR spectroscopy probing millisecond time-scale dynamics in proteins: theory and application. J Am Chem Soc 126:7320–7329. doi:10.1021/ja049968b
Levitt MH, Freeman R (1979) NMR population-inversion using a composite pulse. J Magn Reson 33:473–476. doi:10.1016/0022-2364(79)90265-8
Lundstrom P, Vallurupalli P, Religa TL, Dahlquist FW, Kay LE (2007) A single-quantum methyl ^{13}C-relaxation dispersion experiment with improved sensitivity. J Biomol NMR 38:79–88. doi:10.1007/s10858-007-9149-7
Luy B (2004) Spin state selectivity and heteronuclear Hartmann-Hahn transfer. J Magn Reson 168:210–216. doi:10.1016/j.jmr.2004.03.005
Millet O, Loria JP, Kroenke CD, Pons M, Palmer AG (2000) The static magnetic field dependence of chemical exchange linebroadening defines the NMR chemical shift time scale. J Am Chem Soc 122:2867–2877. doi:10.1021/ja993511y
Mulder FAA, Skrynnikov NR, Hon B, Dahlquist FW, Kay LE (2001) Measurement of slow (μs-ms) time scale dynamics in protein side chains by ^{15}N relaxation dispersion NMR spectroscopy: application to Asn and Gln residues in a cavity mutant of T4 lysozyme. J Am Chem Soc 123:967–975. doi:10.1021/ja003447g
Neudecker P et al (2012) Structure of an intermediate state in protein folding and aggregation. Science 336:362–366. doi:10.1126/science.1214203
Ottiger M, Delaglio F, Bax A (1998) Measurement of J and dipolar couplings from simplified two-dimensional NMR spectra. J Magn Reson 131:373–378. doi:10.1006/jmre.1998.1361
Palmer AG, Kroenke CD, Loria JP (2001) Nuclear magnetic resonance methods for quantifying microsecond-to-millisecond motions in biological macromolecules. Methods Enzymol 339:204–238. doi:10.1016/S0076-6879(01)39315-1
Religa TL, Kay LE (2010) Optimal methyl labeling for studies of supramolecular systems. J Biomol NMR 47:163–169. doi:10.1007/s10858-010-9419-7
Rennella E, Huang R, Velyvis A, Kay LE (2015) $^{13}CHD_2$-CEST NMR spectroscopy provides an avenue for studies of conformational exchange in high molecular weight proteins. J Biomol NMR 63:187–199. doi:10.1007/s10858-015-9974-z
Rosenzweig R, Kay LE (2014) Bringing dynamic molecular machines into focus by methyl-TROSY NMR. Annu Rev Biochem 83:291–315. doi:10.1146/annurev-biochem-060713-035829
Schleucher J, Sattler M, Griesinger C (1993) Coherence selection by gradients without signal attenuation: application to the 3-dimensional HNCO experiment. Angew Chem Int Ed 32:1489–1491. doi:10.1002/anie.199314891
Sekhar A, Kay LE (2013) NMR paves the way for atomic level descriptions of sparsely populated, transiently formed biomolecular conformers. Proc Natl Acad Sci USA 110:12867–12874. doi:10.1073/pnas.1305688110
Sekhar A, Rumfeldt JAO, Broom HR, Doyle CM, Bouvignies G, Meiering EM, Kay LE (2015) Thermal fluctuations of immature SOD1 lead to separate folding and misfolding pathways. Elife 4:e07296. doi:10.7554/eLife.07296
Shaka AJ, Keeler J, Frenkiel T, Freeman R (1983) An improved sequence for broadband decoupling: WALTZ-16. J Magn Reson 52:335–338. doi:10.1016/0022-2364(83)90207-X
Shaka AJ, Lee CJ, Pines A (1988) Iterative schemes for bilinear operators: application to spin decoupling. J Magn Reson 77:274–293. doi:10.1016/0022-2364(88)90178-3
Sheppard D, Sprangers R, Tugarinov V (2010) Experimental approaches for NMR studies of side-chain dynamics in high-molecular-weight proteins. Prog Nucl Magn Reson Spectrosc 56:1–45. doi:10.1016/j.pnmrs.2009.07.004
Sklenar V, Piotto M, Leppik R, Saudek V (1993) Gradient-tailored water suppression for ^{1}H–^{15}N HSQC experiments optimized to retain full sensitivity. J Magn Reson Ser A 102:241–245. doi:10.1006/jmra.1993.1098
Skrynnikov NR, Dahlquist FW, Kay LE (2002) Reconstructing NMR spectra of "invisible" excited protein states using HSQC and HMQC experiments. J Am Chem Soc 124:12352–12360. doi:10.1021/ja0207089
Sprangers R, Kay LE (2007) Quantitative dynamics and binding studies of the 20 S proteasome by NMR. Nature 445:618–622. doi:10.1038/nature05512
Tugarinov V, Kay LE (2005) Methyl groups as probes of structure and dynamics in NMR studies of high-molecular-weight proteins. Chembiochem 6:1567–1577. doi:10.1002/cbic.200500110
Tugarinov V, Kay LE (2007) Separating degenerate ^{1}H transitions in methyl group probes for single-quantum ^{1}H-CPMG relaxation dispersion NMR spectroscopy. J Am Chem Soc 129:9514–9521. doi:10.1021/ja0726456
Tugarinov V, Hwang PM, Ollerenshaw JE, Kay LE (2003) Cross-correlated relaxation enhanced ^{1}H–^{13}C NMR spectroscopy of methyl groups in very high molecular weight proteins and protein complexes. J Am Chem Soc 125:10420–10428. doi:10.1021/ja030153x
Vallurupalli P, Bouvignies G, Kay LE (2012) Studying "invisible" excited protein states in slow exchange with a major state conformation. J Am Chem Soc 134:8148–8161. doi:10.1021/ja3001419
Wuthrich K (1986) NMR of proteins and nucleic acids. Wiley, Hoboken
Yang DW, Kay LE (1999) Improved ^{1}HN-detected triple resonance TROSY-based experiments. J Biomol NMR 13:3–10. doi:10.1023/A:1008329230975
Yang DW, Nagayama K (1996) A sensitivity-enhanced method for measuring heteronuclear long-range coupling constants from the displacement of signals in two 1D subspectra. J Magn Reson Ser A 118:117–121. doi:10.1006/jmra.1996.0017
Yuwen T, Vallurupalli P, Kay LE (2016) Enhancing the sensitivity of CPMG relaxation dispersion to conformational exchange processes by multiple-quantum spectroscopy. Angew Chem Int Ed 55:11490–11494. doi:10.1002/anie.201605843
Yuwen T, Sekhar A, Kay LE (2017) Separating dipolar and chemical exchange magnetization transfer processes in ^{1}H-CEST. Angew Chem Int Ed 56:6122–6125.doi:10.1002/anie.201610759